RESEARCH ARTICLE

Spatial regulation of microtubule disruption during dendrite pruning in *Drosophila*

Svende Herzmann, Ina Götzelmann, Lea-Franziska Reekers and Sebastian Rumpf*

ABSTRACT

Large-scale neurite pruning is an important specificity mechanism during neuronal morphogenesis. *Drosophila* sensory neurons prune their larval dendrites during metamorphosis. Pruning dendrites are severed in their proximal regions, but how this spatial information is encoded is not clear. Dendrite severing is preceded by local breakdown of dendritic microtubules through PAR-1-mediated inhibition of Tau. Here, we investigated spatial aspects of microtubule breakdown during dendrite pruning. Live imaging of fluorescently tagged tubulin shows that microtubule breakdown first occurs at proximal dendritic branchpoints, followed by breakdown at more distal branchpoints, suggesting that the process is triggered by a signal emanating from the soma. In fly dendrites, microtubules are arranged in uniformly oriented arrays where all plus ends face towards the soma. Mutants in kinesin-1 and -2, which are required for uniform microtubule orientation, show defects in microtubule breakdown and dendrite pruning. Our data suggest that the local microtubule organization at branchpoints determines where microtubule breakdown occurs. Local microtubule organization may therefore contribute spatial information for severing sites during dendrite pruning.

KEY WORDS: Dendrite, Pruning, Microtubule, Kinesin, Plus end, *Drosophila melanogaster*

INTRODUCTION

The physiological degeneration of synapses, axons or dendrites without loss of the parent neuron is known as pruning. Pruning is an important developmental mechanism that is used to ensure specificity of neuronal connections and to remove developmental intermediates (Luo and O'Leary, 2005; Schuldiner and Yaron, 2015). Whereas the mechanisms of neurite outgrowth and synapse formation have been studied in some detail, comparably little is known about the mechanisms underlying pruning.

In holometabolous insects, the nervous system is remodeled on a large scale during metamorphosis. In the peripheral nervous system (PNS) of *Drosophila*, several types of sensory neurons undergo either apoptosis or prune their larval processes in an ecdysone-dependent manner. The sensory class IV dendritic arborization (c4da) neurons completely and specifically prune their long and branched larval dendrites at the onset of the pupal phase by a degenerative mechanism, while their axons remain intact (Kuo et al., 2005). Dendrite pruning is induced in a cell-autonomous

fashion by the steroid hormone ecdysone and proceeds in a stereotypical fashion (Kuo et al., 2005; Williams and Truman, 2005). Dendrites are first severed at proximal sites close to the cell body between 5 and 10 h after puparium formation (APF). Severed dendrites are then fragmented and phagocytosed by the epidermal cells surrounding them (Han et al., 2014). First signs of dendrite pruning are visible at 2-3 h APF, when proximal dendrites take on an irregular appearance with beadings and thinnings. In these regions, microtubules are disassembled locally (Lee et al., 2009; Williams and Truman, 2005). Plasma membrane retrieval through increased local endocytosis also contributes to thinning of proximal dendrites (Kanamori et al., 2015). Live imaging and genetic data suggest that local microtubule breakdown precedes membrane thinning (Herzmann et al., 2017; Kanamori et al., 2015). Microtubule disassembly is therefore the earliest known local sign of dendrite pruning. Microtubule disassembly requires the kinase PAR-1, which mediates inhibition of the microtubule-associated protein Tau (Herzmann et al., 2017). Furthermore, dendrite pruning also requires the microtubule-severing enzyme Katanin p60-like 1 (Kat-60L1) (Lee et al., 2009), possibly also downstream of PAR-1 and Tau (Herzmann et al., 2017).

Microtubules are polar rods with so-called 'plus' and 'minus' ends. This nomenclature reflects the fact that the rates of both growth and shrinkage are greater at the plus ends. Microtubules in larval c4da neuron dendrites are oriented uniformly with their plus ends facing the soma ('plus-end-in' orientation) (Rolls et al., 2007; Stone et al., 2008). This uniform orientation is particularly prevalent in the primary and secondary dendrites, while higher order dendrites can also have microtubules with mixed orientation (Ori-McKenney et al., 2012; Yalgin et al., 2015). Uniform dendritic plus-end-in microtubule orientation is known to depend on plus-end-directed motors of the kinesin family (Mattie et al., 2010; Sharp et al., 1997; Yan et al., 2013). In c4da neurons, uniform plus-end-in orientation depends on kinesin-2, which can bind to microtubule plus ends via EB1 and thereby promotes their orientation (Mattie et al., 2010). In *C. elegans*, kinesin-1 was shown to be required for plus-end-in dendritic microtubule orientation (Yan et al., 2013). Kinesin-1 cannot bind to plus ends, and it was suggested that it instead moved wrongly oriented microtubules out of dendrites via microtubule sliding, or that it could be anchored to the dendritic cell cortex and could thus move microtubules out of the dendrite via its motor domain (Yan et al., 2013).

Given that microtubule breakdown occurs very early during the pruning process in a spatially confined manner, it is likely that this process involves spatial cues for pruning, such as the restriction of the destructive process to proximal over distal dendrites, or the sparing of the axon. Here, we addressed the apparent spatial regulation of microtubule disassembly during dendrite pruning by live imaging of fluorescently marked tubulin markers as well as in genetic studies. We found that gaps in dendritic microtubules occur first at proximal dendrite branchpoints and later at more distal ones.

Institute for Neurobiology, University of Münster, Badestrasse 9, 48149 Münster, Germany.

*Author for correspondence (sebastian.rumpf@uni-muenster.de)

S.R., 0000-0002-7128-2645

DEVELOPMENT

We find that kinesin-2 is required for efficient c4da neuron dendrite pruning and microtubule disassembly, and that EB1 manipulation modulates the phenotypes associated with other microtubule disassembly factors, indicating that the uniform plus-end-in orientation of dendritic microtubules is also required for efficient microtubule breakdown and dendrite pruning. This is further supported by our observation that mutation of kinesin-1 also affects dendritic microtubule orientation, disassembly, and dendrite pruning in c4da neurons. We propose that microtubule disassembly depends on a signal emanating from the soma, and that the local microtubule organization at dendrite branchpoints, including the uniform plus-end-in orientation, favors microtubule disassembly there. Our data indicate that dendritic microtubule organization may represent an important spatial cue for severing site selection during dendrite pruning.

RESULTS

Microtubules are first lost at proximal dendritic branchpoints during dendrite pruning

Given that microtubule disassembly is an early and potentially instructive step during c4da neuron dendrite pruning, we wanted to assess the spatial aspects of this process in more detail. We coexpressed fluorescently tagged mCherry::α-tubulin together with the membrane marker CD8::GFP under the control of *pickpocket* (*ppk*)-*GAL4* in c4da neurons and imaged neurons over time during the early pupal phase (Fig. 1A-E). Gaps in the dendritic microtubule signal became visible in proximal dendrites at ∼3-4 h APF, although some dendrites retained continuous mCherry::α-tubulin signal even at 7 h APF. Predominantly, such gaps first occurred at the most proximal dendrite branchpoints of primary dendrites and extended into the smaller side branch (Fig. 1A′-E′,K). Microtubule gaps also developed at the second or higher order branchpoints within a primary branch, but only later, or when the first and second branchpoints were in close proximity (e.g. Fig. 1C′,K). Microtubule gaps starting at branchpoints reached ∼30 μm (N=8) into the smaller dendritic branch (Fig. 1A′-E′).

To assess how quickly microtubule gaps developed, we imaged microtubule loss at 5 min intervals. Complete microtubule loss within a branch region usually occurred within 20-30 min (Fig. 1F′-J′). During this time, the mCherry::α-tubulin signal diminished relatively evenly in proximal stretches of degenerating dendrite branches, with the first gaps often occurring directly at the branchpoints (10/13; Fig. 1F′-J′, Fig. S1). Quantification of the local mCherry::α-tubulin fluorescence showed that the decrease was more pronounced in degenerating than in stable branches and was therefore not due to bleaching (N=13; Fig. S1). Some mCherry::α-tubulin fluorescence could still be detected in the thicker varicosities of degenerating proximal dendrites (Fig. 1F′-J′), which is likely to reflect soluble mCherry::α-tubulin that was not assembled in stable microtubules.

Consistent with the idea of microtubule disassembly as a driver of degeneration during dendrite pruning, the diameter of degenerating dendrites decreased by ∼45% during this time of initial microtubule disassembly in the same samples (Fig. 1L), and varicosities also developed soon after, or even synchronously with, microtubule loss (e.g. Fig. 1F′-J′).

Kinesin-2, but not PAR-1, is required for uniform microtubule orientation in dendrites

The selective occurrence of microtubule loss at branchpoints suggested that the local organization of microtubules in the dendrites could play a role. One particular feature of dendritic microtubules in *Drosophila* is that they are uniformly oriented in a

plus-end-in fashion (Rolls et al., 2007; Stone et al., 2008), in particular in proximal dendrites (Ori-McKenney et al., 2012). To examine whether dendritic microtubule orientation might affect pruning, we set out to identify regulators of dendritic microtubule orientation in c4da neurons. We used a GFP-tagged version of the plus-end-tracking protein EB1 to visualize the movement of microtubule plus ends in dendrites *in vivo*. In control c4da neurons expressing EB1::GFP under the da neuron GAL4 driver $GAL4^{109(2)80}$, EB1::GFP 'comets' moved predominantly in the retrograde direction, indicating a plus-end-in orientation of dendritic microtubules (Fig. 2A,B), as previously described (Rolls et al., 2007; Stone et al., 2008). Kinesin-2 had previously been shown to be required for uniform dendritic microtubule orientation in the fly PNS (Mattie et al., 2010). Downregulation of the regulatory kinesin-2 subunit KAP3 by RNAi led to a significant increase in the percentage of anterogradely moving comets, and hence 'plus-end-out' microtubules (Fig. 2A,B). By contrast, downregulation of the kinase PAR-1 did not cause a change in the directionality of EB1 comets (Fig. 2A,B), indicating that PAR-1 regulates microtubule dynamics, but not microtubule orientation, during dendrite pruning.

We also confirmed the effects of PAR-1 and kinesin-2 manipulation with the kinesin-1 motor domain fusion kinesin-β-galactosidase (Kin-βgal). Kin-βgal binds to microtubules and migrates towards plus ends. Consequently, Kin-βgal is excluded from dendrites and serves as a specific axon marker in c4da neurons (Zheng et al., 2008) (Fig. 2C,C′). In keeping with an altered microtubule orientation upon kinesin-2 manipulation, Kin-βgal could frequently be detected in distal dendrite regions upon *Kap3* RNAi (Fig. 2D,D′), but not upon *par-1* RNAi (Fig. 2E,E′).

Kinesin-2 is required for sensory neuron dendrite pruning and microtubule breakdown during the early pupal phase

In order to test whether the specific microtubule structure of c4da neuron dendrites plays a role during pruning, we next asked whether kinesin-2 is required for dendrite pruning. We downregulated KAP3 expression in c4da neurons by RNAi expressed under control of *ppk-GAL4*. *Kap3* RNAi had little effect on larval c4da neuron morphology (Fig. 3A,B). At 18 h APF, control neurons had pruned all larval dendrites (Fig. 3A′). By contrast, a significant fraction of c4da neurons expressing *Kap3* RNAi retained dendrites, which were somewhat shortened but still attached to the cell body (Fig. 3B′,D,E), indicating an early defect in dendrite severing. We also confirmed this result by assessing the effects of a mutation in *Klp64D*, which encodes a catalytic kinesin-2 subunit. The transheterozygous mutant combination $Klp64D^{n123}/Klp64D^{k1}$ (a likely loss-of-function or strong hypomorph) exhibited very similar dendrite pruning defects at 18 h APF (Fig. 3C′,D,E). Thus, we conclude that kinesin-2 is required for sensory neuron dendrite pruning in the *Drosophila* PNS.

Another factor implicated in uniform dendritic microtubule orientation is EB1 (Mattie et al., 2010). *Eb1* RNAi alone caused only few (∼10%) neurons to retain dendrites attached to the soma at 18 h APF (Fig. 3G,I). In order to explain this apparent lack of any significant defect upon *Eb1* RNAi, we considered that EB1 is known to exert stabilizing effects on neuronal microtubules in addition to its role in microtubule orientation (Yogev et al., 2016). Thus, microtubule destabilization by *Eb1* RNAi might mask a pruning defect through loss of microtubule orientation. We therefore asked whether manipulation of EB1 could modify the pruning defects caused by manipulation of PAR-1. Expression of *par-1* RNAi under *ppk-GAL4* together with a control RNAi caused ∼30% of neurons to retain dendrites attached to the cell body at 18 h
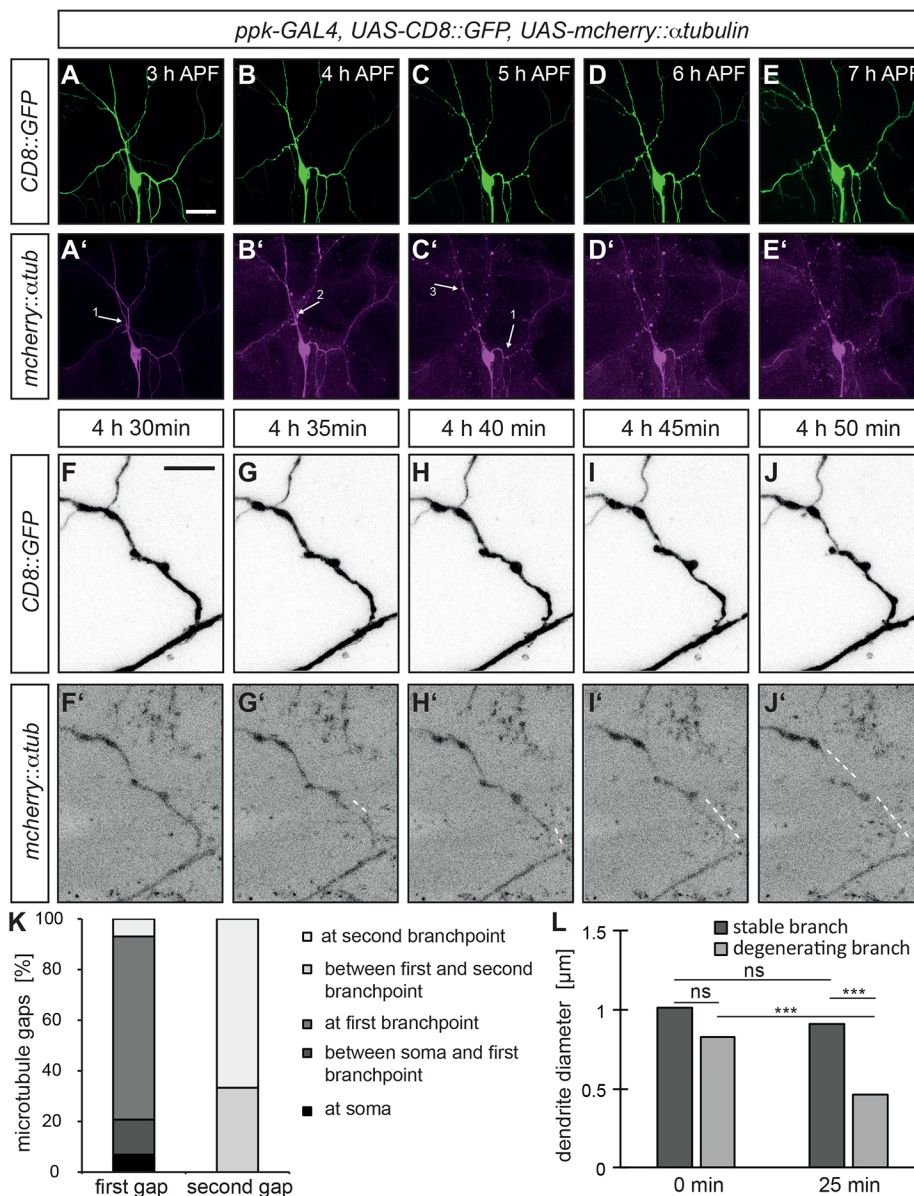
Fig. 1. Spatial aspects of microtubule disassembly during c4da neuron dendrite pruning. (A-E′) Live imaging series of a c4da neuron expressing fluorescently tagged mCherry::αtubulin (A′-E′) and CD8::GFP (A-E, plasma membrane) between 3 and 7 h APF. Numbers (1-3) denote the occurrence and order of gaps in the mCherry::αtubulin signal within the respective primary dendrite branch. (F-J′) Timecourse of microtubule loss in a single dendrite branch. Images of CD8::GFP (F-J) and mCherry::αtubulin (F′-J′) were taken every 5 min starting at 4:30 h APF. Dashed lines (F′-J′) denote an area in the proximal region of the branch where the microtubule signal disappears in a relatively uniform fashion. (K) The distribution of the first and second microtubule gaps in primary c4da neuron dendrites with respect to dendrite landmarks. Data were taken from time-lapse images of c4da neurons as in A-E (N=11 neurons). (L) The diameter of degenerating dendrite branches was measured over a 25 min period, during which microtubule gaps developed (such as in F-J). The diameter of stable branches in the same neurons was taken as the control (N=13 each). ***P>0.0005, Wilcoxon test; ns, not statistically significant. For details of genotypes in this and subsequent figures, see Table S1. Scale bars: 30 μm in A; 10 μm in F.

APF. Intriguingly, coexpression of *par-1* RNAi with *Eb1* RNAi synergistically enhanced these pruning defects to ∼80% (Fig. 3F-I). Strong EB1::GFP overexpression has also been shown to exert mild dominant-negative effects on dendritic microtubule orientation (Mattie et al., 2010). Indeed, EB1::GFP overexpression under a strong *ppk-GAL4* insertion (stronger than the *GAL4^{109(2)80}* used in the EB1::GFP tracking experiments) also led to retention of more dendrite remnants at 18 h APF, indicating a mild delay in dendrite pruning (Fig. S2). Thus, genetic analyses suggest that dendritic microtubule orientation is important for microtubule breakdown during dendrite pruning.

Kinesin-2 is required for microtubule disassembly during dendrite pruning

To address whether uniform microtubule orientation is required for microtubule disassembly during dendrite pruning, we next expressed cherry-tagged α-tubulin (*mCherry::α-tubulin*) under the control of *ppk-GAL4* in *Klp64D^{n123}*/*Klp64D^{k1}* mutant animals and performed time-lapse microscopy as in Fig. 1. *Klp64D^{n123}*/*Klp64D^{k1}* c4da neurons exhibited mostly uninterrupted mCherry::

α-tubulin staining in primary dendrites between 4 and 7 h APF, with only few gaps developing (Fig. 4A-D′).

To confirm these data at the level of endogenous microtubules, we next stained c4da neurons for acetylated α-tubulin at 5 h APF. As such post-translational modifications only accumulate on microtubules, and not on free α-tubulin, they are an indicator of the presence of stable microtubules. Acetylated α-tubulin was lost from proximal dendrites in control c4da neurons (0/7 neurons with continuous acetylated α-tubulin staining; Fig. 4E), but could still be detected at low levels in proximal dendrites of neurons expressing *Kap3* RNAi (3/7 neurons with continuous acetylated α-tubulin staining; Fig. 4F). Thus, kinesin-2, likely through its role in microtubule orientation, is required for microtubule breakdown during dendrite pruning.

Kinesin-1 is required for dendrite pruning

Distinct members of the kinesin family are required for plus-end-in dendritic microtubule orientation in different model organisms, and different mechanisms of action have been proposed (Mattie et al., 2010; Sharp et al., 1997; Yan et al., 2013). It is not clear whether
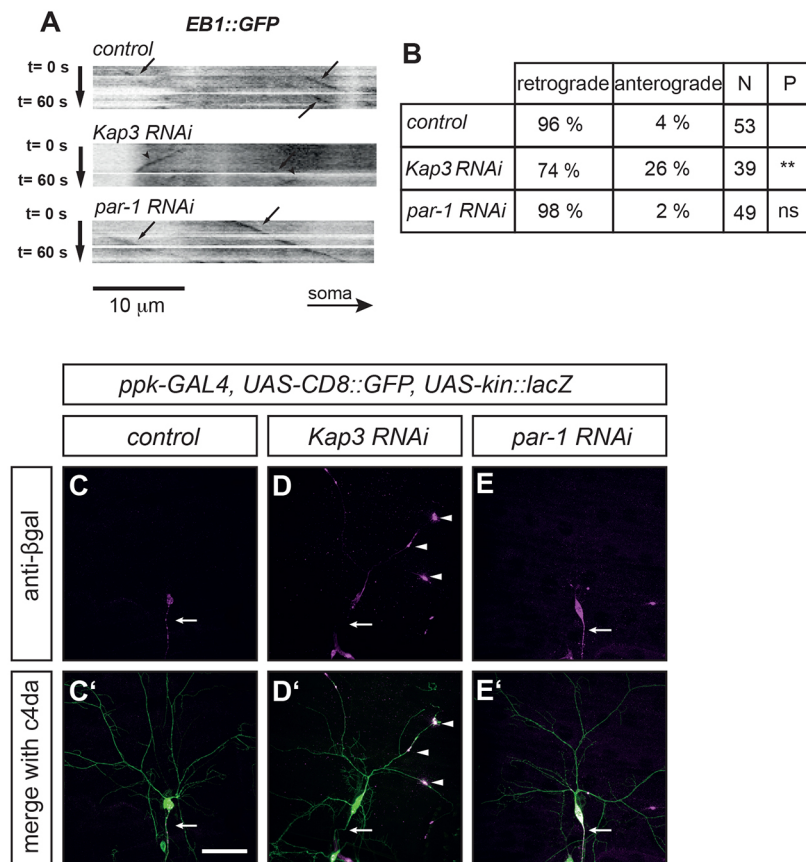
Fig. 2. Uniform microtubule orientation in c4da neuron dendrites depends on kinesin-2, but not PAR-1.
(A) Kymographs of EB1::GFP comets in proximal dendrites of control c4da neurons or those expressing *Kap3* RNAi or *par-1* RNAi. Arrows indicate retrogradely moving EB1::GFP comets; arrowheads indicate EB1::GFP comets moving anterogradely. (B) Summary of the direction of comet movement in EB1 imaging experiments. *N* is the total number of comets per genotype (10 animals each). **$P<0.005$, Fisher's exact test. (C-E′) Localization of the axon marker kinesin-β-galactosidase (Kin-βgal) in control third instar c4da neurons and those expressing *Kap3* RNAi or *par-1* RNAi. β-gal staining (C-E) is merged with CD8::GFP (C′-E′) to show neuronal morphology. Arrows indicate the position of the axon; arrowheads indicate Kin-β-gal accumulations in dendrites. Scale bar: 50 μm.

these findings reflect differences between phyla, or whether several mechanisms of microtubule orientation can co-exist. In *C. elegans*, kinesin-1 was shown to be required for dendritic microtubule orientation (Yan et al., 2013). To address if kinesin-1 is also involved in dendrite pruning, we used *Khc²⁷*, a previously characterized null allele of kinesin-1 heavy chain (Brendza et al., 1999). Heterozygous *Khc²⁷*/+ c4da neurons marked with the promotor fusion *ppk-eGFP* pruned their dendrites normally at 18 h APF (Fig. 5A,A′). However, in mosaic analysis with a repressible cell marker (MARCM) (Lee and Luo, 1999) experiments, homozygous *Khc²⁷* c4da neuron clones still had long and often branched dendrites attached to the soma (Fig. 5B,B′). These defects could be rescued by GAL4/UAS-mediated expression of wild-type KHC in *Khc²⁷* MARCM clones (Fig. 5C-E).

Kinesin-1 is required for microtubule orientation and breakdown

How does kinesin-1 affect dendrite pruning? In order to address whether kinesin-1 is also required for uniform dendritic microtubule orientation, we assessed its effects on the distribution of the axon marker Kin-βgal and the plus end marker EB1::GFP. Consistent with previous work (Yan et al., 2013), we found that Kin-βgal accumulated in dendrites of *Khc²⁷* mutant neurons (Fig. 6A-B′). We next tracked EB1::GFP in proximal dendrites of homozygous *Khc²⁷* c4da neurons. Such MARCM clones displayed a high fraction of anterogradely moving EB1::GFP comets, again indicating a loss of the uniform plus-end-in orientation (Fig. 6C,D).

We next asked whether kinesin-1 is also required for microtubule disassembly during pruning of c4da neuron dendrites. We expressed GFP-tagged α-tubulin in control c4da neurons (under the control of *ppk-GAL4*) or in *Khc²⁷* c4da MARCM clones. At 5 h APF, GFP::

α-tubulin was mostly lost from proximal dendrites in control neurons but persisted in *Khc²⁷* mutant c4da neurons (Fig. 6E-F′). Even though we could only analyze a small number of *Khc²⁷* mutant c4da neurons for acetylated α-tubulin staining at 5 h APF (Fig. 6G), this analysis also indicated the presence of stable microtubules in proximal dendrites (2/2 *Khc²⁷* c4da MARCM clones). Finally, in support of the idea that kinesin-1 is required for microtubule disassembly during dendrite pruning, we also observed that a heterozygous *Khc* mutation (*Khc²⁷*/+) enhanced the pruning defects caused by expression of *par-1* RNAi (Fig. 6H).

These data suggest that both kinesin-1 and kinesin-2 are required for uniform microtubule orientation in c4da neuron dendrites. Kinesin-2 had previously been shown to be required in this system, and it was shown that the underlying mechanism involved direct steering of microtubule plus ends by kinesin-2 (Mattie et al., 2010). In *C. elegans*, the generation of uniform dendritic plus-end-in orientation was attributed to kinesin-1 (Yan et al., 2013). Since kinesin-1 cannot bind to plus ends, it was speculated that it might use microtubule sliding, possibly via its C-terminal microtubule-binding domain (MTBD), to remove wrongly oriented microtubules from dendrites (Yan et al., 2013), or that it could be cortex-anchored and slide microtubules out of dendrites via its motor domain (Kapitein and Hoogenraad, 2015). We assessed the effects of *Khc^MutA*, which lacks the MTBD (Winding et al., 2016), on pruning and microtubule orientation. In c4da neurons, this mutant showed only a very mild and nonsignificant increase in dendritic plus-end-out microtubules, and equally mild pruning defects (Fig. S3), arguing against the MTBD-mediated mechanism in our model system.

Stress induction and activation of the Jun N-terminal kinase (JNK) pathway by axotomy or downregulation of *unc-104*, a synaptic kinesin, has also been shown to increase microtubule
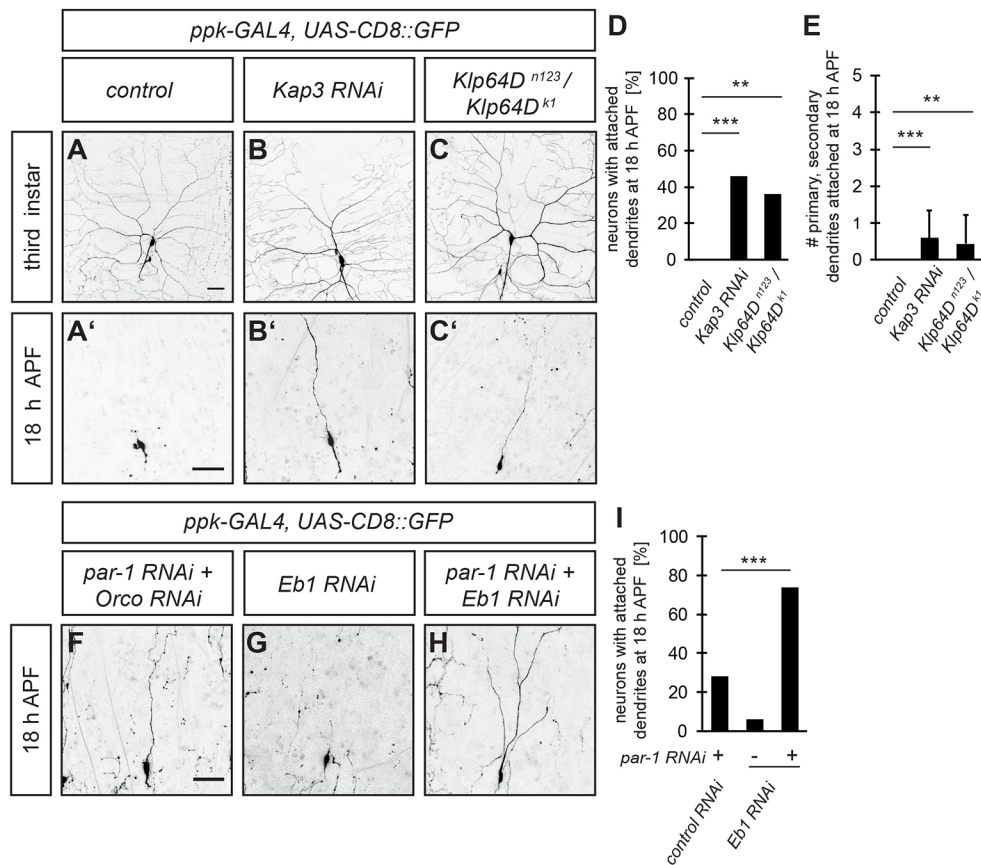
4

Fig. 3. Kinesin-2 is required for c4da neuron dendrite pruning. (A-C′) Loss of kinesin-2 causes defects in c4da neuron dendrite pruning. Neurons are shown at (A-C) third instar or (A′-C′) 18 h APF. (A,A′) Control c4da neurons labeled by CD8::GFP expression under the control of *ppk-GAL4*. (B,B′) c4da neurons expressing *Kap3* RNAi under *ppk-GAL4*. (C,C′) $Klp64D^{n123}/Klp64D^{k1}$ mutant c4da neurons labeled by CD8::GFP expression under *ppk-GAL4*. (D) Percentage of neurons with dendrites attached to the soma at 18 h APF (N=26, 27, 44, respectively, left to right). (E) Number of attached primary and secondary dendrites at 18 h APF. Data are mean±s.d. (F-I) Genetic interactions between EB1 and PAR-1 during dendrite pruning. (F-H) c4da neurons at 18 h APF expressing (F) *par-1* RNAi and *Orco* RNAi as control, (G) *Eb1* RNAi, or (H) both *par-1* RNAi and *Eb1* RNAi. (I) Penetrance of c4da neuron dendrite pruning defects in F-H (N=47, 49, 58, respectively). ***P<0.0005, **P<0.005 by Fisher's exact test (D,I) or Wilcoxon test (E). Scale bars: 50 μm.

dynamics and to change microtubule orientation in dendrites (Chen et al., 2012). Consistently, we found that *unc-104* RNAi causes strong pruning defects (Fig. S4). *unc-104* RNAi also causes other massive stress symptoms, such as strongly decreased GFP marker fluorescence (Fig. S4), which are not seen in the kinesin-1 mutant to the same extent, suggesting that kinesin-1 mutation does not cause microtubule orientation and pruning defects indirectly via stress signaling.

We also noted that the pruning defects seen in the *Khc* mutant were more severe than those observed upon kinesin-2 inactivation.
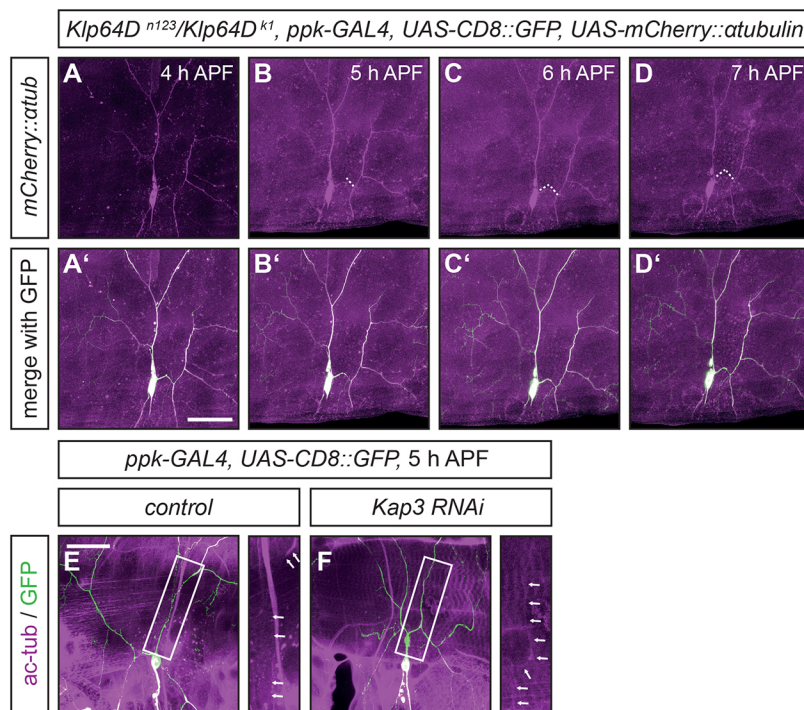

Fig. 4. Kinesin-2 downregulation leads to delays in microtubule breakdown during dendrite pruning. (A-D′) $Klp64D^{n123}/Klp64D^{k1}$ mutant c4da neuron microtubules were labeled by expression of UAS-mCherry::α-tubulin under *ppk-GAL4*, and neuronal morphology was visualized by UAS-CD8GFP. Timecourse imaging between 4 and 7 h APF was performed as in Fig. 1. The mCherry::α-tubulin signal (A-D) is shown merged with the CD8::GFP membrane marker (A′-D′). Dotted lines (B-D) indicate dendrite regions with disrupted microtubules. (E,F) Persistence of microtubules upon KAP3 knockdown. Stable microtubules were labeled with antibody against acetylated α-tubulin at 5 h APF, and c4da neuron morphology was visualized by UAS-CD8GFP expressed under *ppk-GAL4*. (E) Control c4da neuron. (F) c4da neuron expressing *Kap3* RNAi under *ppk-GAL4*. Acetylated α-tubulin staining is merged with GFP staining to delineate c4da neuron morphology. The boxed regions are shown at higher magnification to the right, with acetylated α-tubulin staining only. Arrows indicate the position of c4da neuron dendrites. Scale bars: 50 μm.
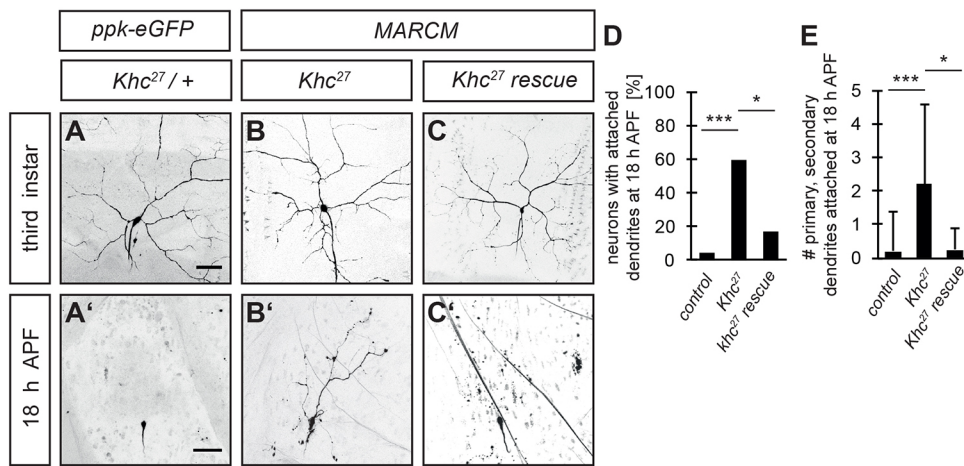
Fig. 5. Kinesin-1 is required for c4da neuron dendrite pruning. (A-C′) c4da neurons of the indicated genotypes are shown at the third instar larval stage (A-C) and at 18 h APF (A′-C′). (A,A′) Heterozygous Khc^{27}/+ control c4da neurons labeled by *ppk-eGFP*. (B,B′) Khc^{27} c4da neuron MARCM clones. (C,C′) Khc^{27} MARCM mutant c4da neurons expressing UAS-GFP::KHC. (D) Percentage of neurons in A′-C′ with attached dendrites (N=26, 13, 12, respectively). (E) Number of attached primary and secondary dendrites at 18 h APF in A′-C′. Data are mean±s.d. ***P<0.0005, *P<0.05 by Fisher's exact test (D) or Wilcoxon test (E).

In addition to the higher penetrance of pruning defects in the Khc^{27} mutant cells, dendrites of c4da neurons lacking KHC were also frequently still branched at 18 h APF, whereas neurons lacking kinesin-2 mostly had only one major branch still attached to the cell body at this time point (Fig. 5B′, Fig. 3B′,C′). It was previously shown in *C. elegans* that kinesin-1 mutation affects neuronal microtubule dynamics (Yogev et al., 2016), in addition to microtubule orientation. The difference in severity between the
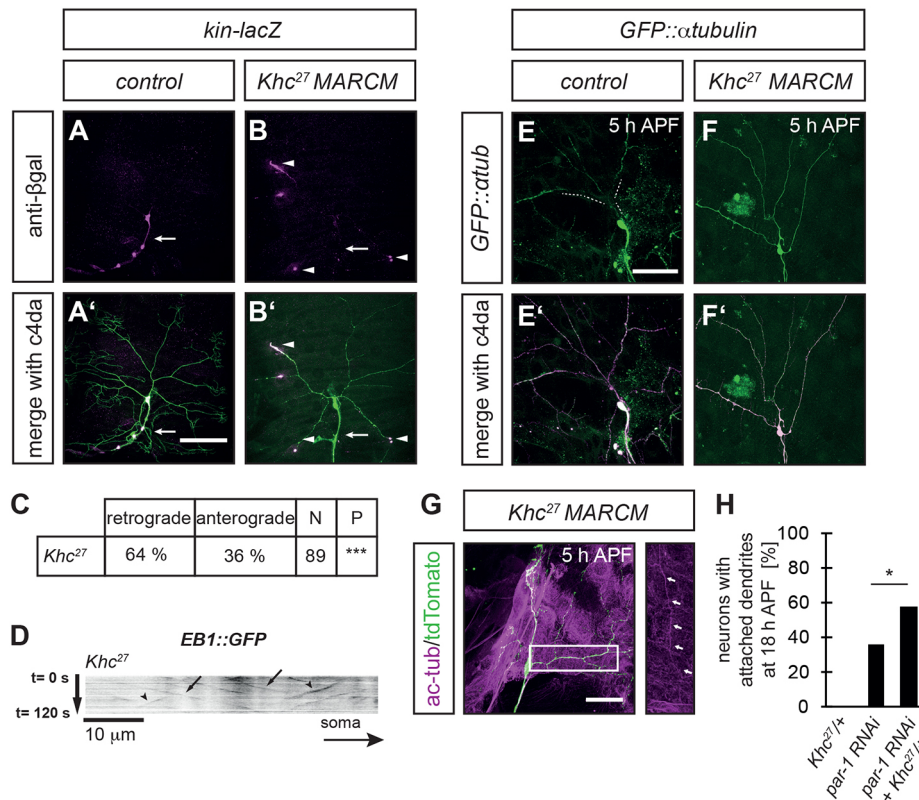

Fig. 6. Kinesin-1 is required for dendritic microtubule orientation and microtubule breakdown during dendrite pruning. (A-B′) Mislocalization of the axon marker Kin-βgal in *Khc* mutant c4da neurons. (A,A′) Control c4da neuron marked by *ppk-GAL4*. (B,B′) Khc^{27} mutant c4da neuron MARCM clone. β-gal staining (A,B) is shown merged with the neuron markers CD8::GFP and Tdtomato, respectively, (A′,B′). Arrows indicate the position of axons and arrowheads indicate dendritic Kin-βgal accumulations. (C,D) Kinesin-1 is required for uniform dendritic microtubule orientation. UAS-EB1::GFP was expressed in control c4da neurons or Khc^{27} c4da MARCM clones, and EB1 comets were tracked in third instar larval proximal dendrites. (C) Quantification of EB1::GFP comet directionality in Khc^{27} mutant neurons. ***P<0.0005, Fisher's exact test. (D) Representative 2 min kymograph of EB1::GFP comets. The direction of the soma is indicated. Arrows and arrowheads indicate retrograde and anterograde comets, respectively. (E,F) c4da neuron microtubules at 5 h APF were labeled by expression of UAS-GFP::α-tubulin under *ppk-GAL4*, and neuronal morphology was visualized by UAS-tdTomato. GFP::α-tubulin staining (E,F) is shown merged with tdTomato (E′,F′) for control (E,E′) and Khc^{27} mutant MARCM (F,F′) c4da neurons. Dashed lines (E) indicate dendrite regions that have lost GFP::α-tubulin staining. (G) Stable microtubules in a Khc^{27} mutant MARCM c4da neuron were visualized with an antibody against acetylated α-tubulin as in Fig. 4E,F. Acetylated α-tubulin staining is merged with tdTomato to delineate c4da neuron morphology. The boxed region is shown at higher magnification to the right, with acetylated α-tubulin staining only. Arrows indicate the position of c4da neuron dendrites. (H) Heterozygosity for Khc^{27} enhances the pruning defects caused by PAR-1 knockdown. Pruning defects of the indicated genotypes were scored as in Fig. 2. *P<0.05, Fisher's exact test. N=31, Khc^{27}/+; N=84, *par-1* RNAi; N=95, Khc^{27}/+ plus *par-1* RNAi. See also Figs S1 and S2. Scale bars: 50 μm.

pruning defects in the kinesin-1 mutant and upon kinesin-2 manipulations is likely to be due to the twofold effect of kinesin-1 on both dendritic microtubule orientation and stability. Thus, our data suggest that several kinesin-based mechanisms might operate at the same time to achieve microtubule uniformity.

Taken together, our results indicate that the uniform plus-end-in microtubule organization in c4da neuron dendrites is required for efficient microtubule breakdown and subsequent dendrite pruning during the early pupal phase.

DISCUSSION

Microtubule disassembly is the earliest known local destabilizing process during c4da neuron dendrite pruning and therefore a likely candidate to determine proximal severing. In this study, we have begun to address the spatial regulation of microtubule disassembly during c4da neuron dendrite pruning. Using time-lapse live imaging of fluorescently tagged tubulin, we found that gaps in the fluorescent microtubule signal develop preferentially at branchpoints of primary dendrites, and usually extend into the smaller side branches, rather than in the primary branch (Fig. 1). Moreover, the temporal occurrence of these gaps correlates with proximity to the soma, i.e. microtubule gaps initially develop at the first branchpoint and later at the more distal branchpoints. These observations are consistent with a microtubule-destabilizing signal emanating from the soma. We previously showed that microtubule disassembly is induced by PAR-1-mediated Tau inhibition (Herzmann et al., 2017). PAR-1 activity is often induced by phosphorylation. Our previous data suggested that PAR-1 is specifically activated for microtubule disassembly at the onset of the pupal phase, possibly by ecdysone (Herzmann et al., 2017). It is therefore plausible that the signal emanating from the soma is activated PAR-1. In such a model, activation of PAR-1 in the soma would contribute to the preference for microtubule disruption (and later dendrite severing) in proximal dendrites (Fig. 7A).

We also found that the uniform plus-end-in orientation of dendritic microtubules is required for efficient microtubule disassembly and dendrite pruning (e.g. Figs 2 and 3). We found that kinesin-2 and kinesin-1, both affecting dendritic microtubule orientation, are required for dendrite pruning. Manipulation of EB1, which caused less severe dendrite pruning defects by itself, strongly modified the defects seen upon manipulation of the microtubule dynamics regulator PAR-1. Interestingly, microtubule orientation (and hence the localization of the outermost microtubule plus ends) correlates well with the sites of degeneration and the degeneration mode in several models of large-scale pruning (Fig. 7B). For example, degeneration often starts from the distal end in axons, where microtubules have uniform plus-end-out orientation. As in c4da neurons (Herzmann et al., 2017; Kanamori et al., 2015), microtubule disassembly is an early event during large-scale axon pruning and is therefore likely to carry intrinsic spatial information crucial for pruning as well. This was shown to be the case in pruning axons of *Drosophila* mushroom body γ neurons (Watts et al., 2003) and for pruning motoneuron axons at the mammalian neuromuscular junction (Brill et al., 2016). These axons retract, i.e. they shrink from their distal ends. Intriguingly, and in an exactly opposite manner to c4da neuron dendrites, these axons degenerate from the distal tips, and degeneration stops at the next branchpoint, again implying input from neurite branchpoints in the spatial regulation of large-scale pruning (Brill et al., 2016; Watts et al., 2003).

What could be special about microtubules at branchpoints? Although branchpoints could be localization sites for spatial
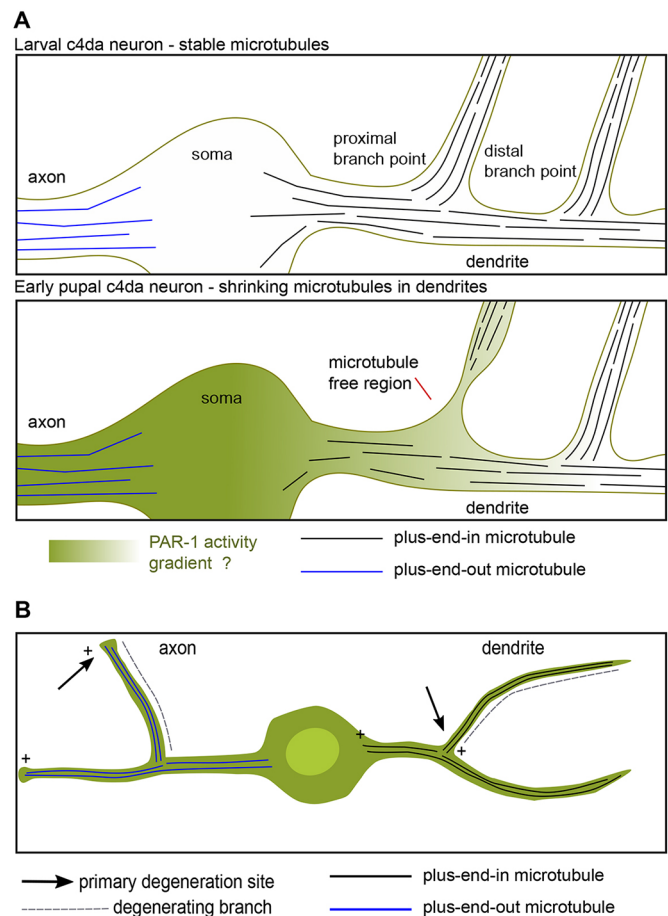

Fig. 7. Model for microtubule-based coding of spatial information during large-scale dendrite pruning. (A) Model for microtubule disassembly during c4da neuron dendrite pruning. Depicted are uniformly plus-end-in oriented microtubules and a putative gradient of a microtubule destabilizer such as PAR-1. (B) Correlation between microtubule orientation and sites of degeneration and degeneration mode in neurites. Whereas dendritic branches with plus-end-in microtubules start to degenerate in their proximal regions, axonal branches (e.g. of vertebrate motoneurons or mushroom body neurons) with plus-end-out microtubules degenerate or retract from distal ends or synapses.

pruning regulators, it is interesting to speculate that the local microtubule organization at branchpoints might suffice. For dendrites, uniformly oriented microtubules within the microtubule array would presumably enable the formation of larger gaps if the plus ends of the array microtubules have similar positions (Fig. 7A). Alternatively, microtubules at branchpoints could be more likely to be bent, and might therefore be more susceptible to shrinkage or catastrophe (Odde et al., 1999). Also, the overlap between the microtubule arrays of the primary and side branches may be smaller than that within an array in a straight branch, enabling gaps to occur at these sites even with relatively little microtubule shrinkage. Of note, our previous data suggest that PAR-1 acts through inhibition of Tau to promote microtubule breakdown (Herzmann et al., 2017), and Tau was recently shown to promote microtubule bundling (Hernandez-Vega et al., 2017). Thus, PAR-1 activation might lead to 'unbundling' of microtubules at branchpoints. Furthermore, it could also be speculated that local concentrations of activated PAR-1 might increase as the diameter of the dendrite side branch decreases, which would also favor microtubule disassembly at proximal branchpoints. In order to distinguish between these

models, it will be important to better characterize the local microtubule organization at dendritic branchpoints.

We and others have previously proposed that microtubule disassembly acts upstream of membrane thinning (Herzmann et al., 2017; Kanamori et al., 2015). We observed dendrite thinning to ~55% during the time of microtubule breakdown (Fig. 1L). Importantly, dendrites can often thin out to ~20% of their original diameter before rupturing (Kanamori et al., 2015), indicating that microtubule loss correlates with the onset of dendrite thinning.

Taken together, our data reveal that the spatial regulation of neurite pruning depends on the local microtubule organization. Our data are consistent with a model in which microtubule disassembly carries the spatial information for pruning and therefore contributes to the selection of both degeneration mode and severing sites.

MATERIALS AND METHODS

Fly stocks and culture
All crosses were performed at 25°C under standard conditions. For expression in c4da neurons, we used *ppk-GAL4* insertions on the second and third chromosomes, and *GAL4^{109(2)80}* for EB1::GFP analysis. MARCM clones of *Khc^{27}* mutants were induced with *SOP-FLP* (Matsubara et al., 2011) and labeled by tdTomato expression under *nSyb-GAL4^{R57C10}* (BL #39171). Other fly lines were *Klp64D^{n123}* (BL #5674), *Klp64D^{k1}* (BL #5578), UAS-GFP::α-tubulin (BL #7373), UAS-mCherry::α-tubulin (BL #25774), UAS-EB1::GFP (Zheng et al., 2008), UAS-kin::lacZ (Clark et al., 1997), UAS-GFP::KHC (Schmidt et al., 2012), UAS-tdTomato (Han et al., 2014) and UAS-dcr2 (Dietzl et al., 2007). UAS-RNAi lines were: *par-1* (BL #32410), *Kap3* (VDRC 103548), *Eb1* (VDRC 24451) and *unc-104* (VDRC 23465). A list of the experimental genotypes for all figures is provided in Table S1.

Dissection, microscopy and live imaging
Microtubule breakdown was followed by imaging UAS-mCherry::α-tubulin (and UAS-CD8::GFP to mark membranes) expressed under the control of *ppk-GAL4*. Pupae were attached to coverslips with heptane glue and selected c4da neurons (segments A2-A5) were imaged in 30-60 min intervals between 2 and 7 h APF, or in 5 min intervals between 3 and 5 h APF using a Zeiss LSM710 or LSM880 confocal microscope. Where necessary, background from the pupal case in live imaging stacks was removed using the surface masking function of Imaris (Bitplane) in a manner that did not affect the actual signal intensity of fluorescent reporters.

Pruning defects were assayed at 18 h APF as described (Rumpf et al., 2014), and analyzed using an LSM710 confocal microscope. For *par-1* genetic interactions, candidates were crossed to a second chromosome insertion of *ppk-GAL4* combined with *UAS-CD8GFP* and *UAS-par-1 RNAi*. EB1::GFP imaging was performed as described (Zheng et al., 2008) using an LSM880 confocal microscope.

Pruning phenotypes were analyzed by counting the number of neurons that still had dendrites attached to the soma; these data were analyzed using a two-tailed Fisher's exact test. In order to measure the severity of pruning defects, we counted the number of primary and secondary branches still attached to the soma at 18 h APF; these data were analyzed using the Wilcoxon-Mann-Whitney test.

Antibodies and immunohistochemistry
Larval or pupal filets were dissected quickly and fixed in PBS containing 4% formaldehyde for 20 min at room temperature. Filets were permeabilized in PBS with 0.3% Triton X-100 and blocked in PBS containing 0.3% Triton X-100 and 10% goat serum. The following primary antibodies were added in blocking solution overnight at 4°C: mouse anti-GFP (Life Technologies, 3E6; 1:1000), chicken anti-GFP (Aves Labs, GFP-1020; 1:500), rabbit anti-DsRed (Clontech Living Colors, 632496; 1:1000), rat anti-mCherry (Life Technologies, 11217; 1:1000), mouse anti-acetylated tubulin (Sigma, 7451; 1:1000) and rabbit anti-β-galactosidase (Cappel, preabsorbed in-house; 1:100). Samples were then incubated with

appropriate Alexa Fluor-conjugated secondary antibodies (Invitrogen) overnight at 4°C, and mounted in Vectashield mounting medium (Vector Laboratories) after three washes in PBS with 0.3% Triton X-100. Images were processed as maximum projections in ImageJ (NIH). For anti-acetylated tubulin stainings, stacks with strong background signal from adjacent epidermal cells were excluded.

References
Brendza, K. M., Rose, D. J., Gilbert, S. P. and Saxton, W. M. (1999). Lethal kinesin mutations reveal amino acids important for ATPase activation and structural coupling. *J. Biol. Chem.* **274**, 31506-31514.

Brill, M. S., Kleele, T., Ruschkies, L., Wang, M., Marahori, N. A., Reuter, M. S., Hausrat, T. J., Weigand, E., Fisher, M., Ahles, A. et al. (2016). Branch-specific microtubule destabilization mediates axon branch loss during neuromuscular synapse elimination. *Neuron* **92**, 845-856.

Chen, L., Stone, M. C., Tao, J. and Rolls, M. M. (2012). Axon injury and stress trigger a microtubule-based neuroprotective pathway. *Proc. Natl. Acad. Sci. USA* **109**, 11842-11847.

Clark, I. E., Jan, L. Y. and Jan, Y. N. (1997). Reciprocal localization of Nod and kinesin fusion proteins indicates microtubule polarity in the Drosophila oocyte, epithelium, neuron and muscle. *Development* **124**, 461-470.

Dietzl, G., Chen, D., Schnorrer, F., Su, K.-C., Barinova, Y., Fellner, M., Gasser, B., Kinsey, K., Oppel, S., Scheiblauer, S. et al. (2007). A genome-wide transgenic RNAi library for conditional gene inactivation in Drosophila. *Nature* **448**, 151-156.

Han, C., Song, Y., Xiao, H., Wang, D., Franc, N. C., Jan, L. Y. and Jan, Y.-N. (2014). Epidermal cells are the primary phagocytes in the fragmentation and clearance of degenerating dendrites in Drosophila. *Neuron* **81**, 544-560.

Hernández-Vega, A., Braun, M., Scharrel, L., Jahnel, M., Wegmann, S., Hyman, B. T., Alberti, S., Diez, S. and Hyman, A. A. (2017). Local nucleation of microtubule bundles through tubulin concentration into a condensed tau phase. *Cell Rep.* **20**, 2304-2312.

Herzmann, S., Krumkamp, R., Rode, S., Kintrup, C. and Rumpf, S. (2017). PAR-1 promotes microtubule breakdown during dendrite pruning in Drosophila. *EMBO J.* **36**, 1981-1991.

Kanamori, T., Yoshino, J., Yasunaga, K.-I., Dairyo, Y. and Emoto, K. (2015). Local endocytosis triggers dendritic thinning and pruning in Drosophila sensory neurons. *Nat. Commun.* **6**, 6515.

Kapitein, L. C. and Hoogenraad, C. C. (2015). Building the neuronal microtubule cytoskeleton. *Neuron* **87**, 492-506.

Kuo, C. T., Jan, L. Y. and Jan, Y. N. (2005). Dendrite-specific remodeling of Drosophila sensory neurons requires matrix metalloproteases, ubiquitin-proteasome, and ecdysone signaling. *Proc. Natl. Acad. Sci. USA* **102**, 15230-15235.

Lee, T. and Luo, L. (1999). Mosaic analysis with a repressible cell marker for studies of gene function in neuronal morphogenesis. *Neuron* **22**, 451-461.

Lee, H.-H., Jan, L. Y. and Jan, Y.-N. (2009). Drosophila IKK-related kinase Ik2 and Katanin p60-like 1 regulate dendrite pruning of sensory neuron during metamorphosis. *Proc. Natl. Acad. Sci. USA* **106**, 6363-6368.

Luo, L. and O'Leary, D. D. M. (2005). Axon retraction and degeneration in development and disease. *Annu. Rev. Neurosci.* **28**, 127-156.

Matsubara, D., Horiuchi, S.-Y., Shimono, K., Usui, T. and Uemura, T. (2011). The seven-pass transmembrane cadherin Flamingo controls dendritic self-avoidance via its binding to a LIM domain protein, Espinas, in Drosophila sensory neurons. *Genes Dev.* **25**, 1982-1996.

Mattie, F. J., Stackpole, M. M., Stone, M. C., Clippard, J. R., Rudnick, D. A., Qiu, Y., Tao, J., Allender, D. L., Parmar, M. and Rolls, M. M. (2010). Directed microtubule growth, +TIPs, and kinesin-2 are required for uniform microtubule polarity in dendrites. *Curr. Biol.* **20**, 2169-2177.

Odde, D. J., Ma, L., Briggs, A. H., DeMarco, A. and Kirschner, M. W. (1999). Microtubule bending and breaking in living fibroblast cells. *J. Cell Sci.* **112**, 3283-3288.

Ori-McKenney, K. M., Jan, L. Y. and Jan, Y.-N. (2012). Golgi outposts shape dendrite morphology by functioning as sites of acentrosomal microtubule nucleation in neurons. *Neuron* **76**, 921-930.

Rolls, M. M., Satoh, D., Clyne, P. J., Henner, A. L., Uemura, T. and Doe, C. Q. (2007). Polarity and intracellular compartmentalization of Drosophila neurons. *Neural Dev.* **2**, 7.

Rumpf, S., Bagley, J. A., Thompson-Peer, K. L., Zhu, S., Gorczyca, D., Beckstead, R. B., Jan, L. Y. and Jan, Y. N. (2014). Drosophila valosin-containing protein is required for dendrite pruning through a regulatory role in mRNA metabolism. *Proc. Natl. Acad. Sci. USA* **111**, 7331-7336.

Schmidt, I., Thomas, S., Kain, P., Risse, B., Naffin, E. and Klämbt, C. (2012). Kinesin heavy chain function in Drosophila glial cells controls neuronal activity. *J. Neurosci.* **32**, 7466-7476.

Schuldiner, O. and Yaron, A. (2015). Mechanisms of developmental neurite pruning. *Cell. Mol. Life Sci.* **72**, 101-119.

Sharp, D. J., Yu, W., Ferhat, L., Kuriyama, R., Rueger, D. C. and Baas, P. W. (1997). Identification of a microtubule-associated motor protein essential for dendritic differentiation. *J. Cell Biol.* **138**, 833-843.

Stone, M. C., Roegiers, F. and Rolls, M. M. (2008). Microtubules have opposite orientation in axons and dendrites of Drosophila neurons. *Mol. Biol. Cell* **19**, 4122-4129.

Watts, R. J., Hoopfer, E. D. and Luo, L. (2003). Axon pruning during Drosophila metamorphosis: evidence for local degeneration and requirement of the ubiquitin-proteasome system. *Neuron* **38**, 871-885.

Williams, D. W. and Truman, J. W. (2005). Cellular mechanisms of dendrite pruning in Drosophila: insights from in vivo time-lapse of remodeling dendrite arborizing sensory neurons. *Development* **132**, 3631-3642.

Winding, M., Kelliher, M. T., Lu, W., Wildonger, J. and Gelfand, V. I. (2016). Role of kinesin-1-based microtubule sliding in Drosophila nervous system development. *Proc. Natl. Acad. Sci. USA* **113**, E4985-E4994.

Yalgin, C., Ebrahimi, S., Delandre, C., Yoong, L. F., Akimoto, S., Tran, H., Amikura, R., Spokony, R., Torben-Nielsen, B., White, K. P. et al. (2015). Centrosomin represses dendrite branching by orienting microtubule nucleation. *Nat. Neurosci.* **18**, 1437-1445.

Yan, J., Chao, D. L., Toba, S., Koyasako, K., Yasunaga, T., Hirotsune, S. and Shen, K. (2013). Kinesin-1 regulates dendrite microtubule polarity in Caenorhabditis elegans. *eLife* **2**, e00133.

Yogev, S., Cooper, R., Fetter, R., Horowitz, M. and Shen, K. (2016). Microtubule organization determines axonal transport dynamics. *Neuron* **92**, 449-460.

Zheng, Y., Wildonger, J., Ye, B., Zhang, Y., Kita, A., Younger, S. H., Zimmerman, S., Jan, L. Y. and Jan, Y. N. (2008). Dynein is required for polarized dendritic transport and uniform microtubule orientation in axons. *Nat. Cell Biol.* **10**, 1172-1180.

DEVELOPMENT